JGR Space Physics

RESEARCH ARTICLE
10.1029/2020JA028210

Nighttime Ionospheric TEC Study Over Latin America During Moderate and High Solar Activity

E. Romero-Hernandez[1,2], C. M. Denardini[2], O. F. Jonah[3], P. Essien[2], G. A. S. Picanço[2], P. A. B. Nogueira[4], M. Rodriguez-Martinez[5], L. C. A. Resende[2,6], V. de la Luz[5], E. Agular-Rodriguez[7], M. Sergeeva[7,8], J. A. Gonzalez-Esparza[7], H. Takahashi[2], and E. Perez-Tijerina[1]

[1]Facultad de Ciencias Fisico-Matemáticas, Universidad Autónoma de Nuevo León, LANCE, Monterrey, Mexico, [2]Instituto Nacional de Pesquisas Espaciais, São José dos Campos, Brazil, [3]MIT Haystack Observatory, Massachusetts Institute of Technology, Westford, MA, USA, [4]Instituto Federal de Educação, Ciencia e Tecnologia de São Paulo, Jacarei, Brazil, [5]Escuela Nacional de Estudios Superiores, Unidad Morelia, Universidad Nacional Autónoma de México, Mexico City, Mexico, [6]State Key Laboratory of Space Weather, Beijing, China, [7]LANCE, Instituto de Geofísica, Unidad Michoacán, Universidad Nacional Autónoma de México, Morelia, Michoacán, Morelia, Mexico, [8]CONACyT, Instituto de Geofísica, Unidad Michoacan, Universidad Nacional Autónoma de México, Morelia, Mexico

Key Points:
- TEC maps for the Latin American region have been developed as a tool for analyzing the spatial and temporal nighttime ionosphere variations
- The MSNA was analyzed in terms of downward plasma fluxes and equatorward winds registered during January and December
- The seasonal variability of the ionosphere over this region, including the EIA and the MSNA, became no longer significant after midnight

Supporting Information:
- Table S1
- Figure S1
- Figure S2

Correspondence to:
E. Romero-Hernandez
and C. M. Denardini,
esmeralda.romerohdz@uanl.edu.mx;
clezio.denardin@inpe.br

Citation:
Romero-Hernandez, E., Denardini, C. M., Jonah, O. F., Essien, P., Picanço, G. A. S., Nogueira, P. A. B., et al. (2020). Nighttime ionospheric TEC study over Latin America during moderate and high solar activity. *Journal of Geophysical Research: Space Physics*, *125*, e2020JA028210. https://doi.org/10.1029/2020JA028210

Received 7 MAY 2020
Accepted 18 AUG 2020
Accepted article online 22 AUG 2020

Abstract The present work is a comprehensive study of the ionospheric vertical total electron content (vTEC) variations during the nighttime, based on data collected by ground-based Global Navigation Satellite System (GNSS) receivers over the Latin American region. We provide a qualitative and quantitative analysis of the ionospheric vTEC trend at 21:00, 00:00, and 03:00 local time (LT), during geomagnetically undisturbed days of 2011 (ascending phase) and 2014 (maximum phase), which encompassed (a) the response to the solar flux variation, (b) the seasonal trend in different latitudes and longitudes, and (c) the interhemispheric asymmetry. One significant result of this study is the development of TEC maps for the Latin American region, which are used for the monitoring and forecasting of the ionosphere for space weather purposes. The nighttime vTEC variations showed a strong latitudinal dependence, especially in the Northern Hemisphere. For 2011, the semiannual anomaly was similar to that observed in daytime; however, in 2014, the receivers at midlatitude presented asymmetric behavior. Similarly, the nighttime winter anomaly (NWA) was very weak in both years. The Equatorial Ionospheric Anomaly (EIA) signature was absent from June to August, a period in which the hemispheric disparity in the vTEC values became more evident, suggesting a feeble interhemispheric circulation. The Midlatitude Summer Nighttime Anomaly (MSNA) was also identified in the Southern Hemisphere, during January and February of 2011 (moderate solar activity). Model approximations suggest that the equatorward winds and the EIA were involved in the formation of the MSNA.

1. Introduction

The ionospheric electron density depends on the solar electromagnetic radiation (EUV and X-ray), the neutral composition, and dynamical effects of neutral winds and electric fields (Buonsanto, 1999). During the daytime, the electron density variation is mainly attributed to changes in the neutral composition ($[O]/[N_2]$ ratio), related in turn to the photoionization rate and low atmospheric processes (e.g., neutral winds and wave-like disturbances). Nonetheless, at night, the photoionization becomes less significant, and the thermospheric processes are assumed to play a major role in the time evolution of the ionospheric electron density profile (Balan et al., 2000; Unnikrishnan et al., 2002, 2006). From this perspective, few works have studied the nighttime seasonal variation of the electron density, as well as its dependence on the solar activity cycle. For instance, Balan et al. (2000) investigated the seasonal and annual variations of the electron density at different altitudes by using data from the middle and upper atmosphere (MU) radar located in Shigaraki, Japan, from 1986 to 1994. They found out that, in general, the variability of the ionosphere has a strong dependence on the altitude. In addition, Chen et al. (2008) analyzed the solar activity dependence on the nighttime ionospheric peak electron density (N_mF_2) by considering different seasons and latitudes. They observed seasonal differences and a linear dependence of N_mF_2 with the solar activity variation in the nighttime, particularly at equinoctial months.

In events related to solar activity, such as solar flares and geomagnetic storms, the variability of the ionosphere is much higher, which results in the formation of ionospheric disturbances (Buonsanto, 1999; Fuller-Rowell et al., 1997; Rishbeth & Mendillo, 2001). During solar flares, the electron density becomes higher because of the ionization enhancement caused by the increase of solar flux emission. In a geomagnetic storm event, the geomagnetic field is highly variable, affecting the currents flowing through the magnetosphere and the ionosphere, and hence, the composition and dynamics of the ionosphere and thermosphere are also affected. Thus, the day-to-day variability of the ionosphere is linked to solar activity, and the ionospheric studies must separately consider quiet and disturbed periods.

The other important ionospheric feature is the equatorial ionization anomaly (EIA), which results from a combination of vertical plasma drift ($\vec{E}\times\vec{B}$) and transport mechanisms (Balan et al., 2018). In simple terms, this anomaly is caused by the plasma movement (vertical plasma drift) to high altitudes, which eventually is dispersed along the magnetic field lines to low latitudes by the action of gravity and pressure gradients (the plasma fountain effect). Thus, the signatures of EIA are two crests of electron density located around ±15°. This feature is predominantly observed on the dayside. During the evening period, however, the vertical plasma drift is also due to the interaction between thermospheric zonal wind and the gradient of Pederson conductivity of the E layer across the solar terminator (Abdu, 2005). Such enhancement of the vertical plasma drift, known as a prereversal enhancement (PRE), generates the development of EIA structure. In addition, an important longitudinal variability of the EIA has been reported at nighttime, which has been associated with the change of vertical plasma drift magnitude (e.g., Lin et al., 2007). Some works have also pointed out that this ionospheric variability is linked to mesospheric processes such as lower atmospheric waves (Fang et al., 2013; H. L. Liu et al., 2013; Rishbeth & Mendillo, 2001). For the lower thermosphere, gravity waves can produce the bottomside disturbance that, in turn, induces the layer instability (e.g., Fritts et al., 2013).

The variability of the ionosphere has been studied using the radio occultation technique, ionosonde data, model simulations, and total electron content (TEC) measurements. In the case of TEC measurements, the wide distribution of the GNSS receivers allows monitoring the ionosphere at different latitudes and longitudes with a high temporal resolution. For that reason, many different works based on TEC measurements have been developed to determine the morphological features of the ionophere over numerous regions. For example, Tsai et al. (2001) studied the seasonal variability over the Asian EIA. In the same way, Rama Rao et al. (2006) analyzed the ionosphere variations on the Indian region during low solar activity. L. Liu et al. (2009) used global ionospheric maps to study the electron density variations associated with the solar cycle activity, at different latitudes. Jonah et al. (2015) investigated TEC variations over South America in both low and high solar activity. More recently, Sergeeva et al. (2018) also studied the TEC behavior over the Mexican region. All these works have shown different aspects of the TEC behavior in these regions; however, there are still more aspects to study, especially at nighttime.

In addition, based on the density peak of the F_2 layer (N_mF_2) and the TEC measurements, some anomalies such as annual and semiannual anomalies, the nighttime winter anomaly (NWA), and the Midlatitude Summer Nighttime Anomaly (MSNA), have been reported at nighttime (e.g., Sai Gowtam & Tulasi Ram, 2017; Jakowski et al., 2015; Lee et al., 2011; H. L. Liu et al., 2013; Tsugawa et al., 2007). The annual anomaly is a global feature in which, by combining the Northern and Southern Hemispheres, a higher electron density is observed during the December solstice rather than in the June solstice (Zhao et al., 2008). The NWA is referred to as the higher mean ionization level in winter nights than in summer (Foster & Jakowski, 1988). Such a feature has been observed during periods of low solar activity, being predominant around geomagnetic midlatitudes (~40–50°). On the other hand, the MSNA is a phenomenon in which nighttime TEC during local summer turns out to be higher than in the daytime. This anomaly can be present in the two hemispheres. Lin et al. (2010) analyzing FORMOSAT-3/COSMIC observations of 2007 (in the descending phase of solar cycle) showed that MSNA is more significant around midnight, especially during January, November, and December. They suggested that an enhanced eastward electric field at the equator (enhanced fountain effect) around 18:00 to 20:00 LT is a necessary condition, in conjunction with equatorward winds, for the formation of MSNA in the Northern and Southern Hemispheres.

Latin America encompasses a region that gathers ionospheric characteristics of equatorial, low, and middle latitudes. Spatial and temporal electron density variations coexist there, as well as more sporadic phenomena. In a previous study, we have analyzed the day-to-day ionosphere variations over Latin America for the

Table 1
On the Left, the Main GNSS Receivers Used for the Comparative vTEC Analysis

receiver	latitude	longitude	mlat	mlon
ACP1	9.4	-79.9	19.7	-8.0
ALUM	-27.3	-66.6	-17.3	5.3
AMMU	-3.4	-57.7	6.2	14.7
ANTC	-37.3	-71.5	-27.2	0.7
AREQ	-16.5	-71.5	-6.4	0.8
AUTF	-54.3	-68.3	-44.2	3.3
CONZ	-37.0	-73.0	-26.7	-0.7
COYQ	-45.5	-71.5	-35.4	0.3
FALK	-51.7	-57.9	-40.7	10.5
IQQE	-21.1	-69.9	-11.1	2.3
LRBR	-10.0	-67.9	0.01	4.4
LMMF	14.6	-61.0	24.1	12.0
MANA	12.2	-86.3	21.7	-14.8
MTNX	-14.7	-52.4	-5.2	19.3
PARC	-53.1	-70.9	-43.0	1.2
POAL	-30.1	-51.1	-20.8	19.5
PUIN	3.9	-67.9	13.7	4.5
RDSD	18.5	-69.9	28.3	2.5
RIOP	-1.5	-78.5	8.2	-6.5
RIO2	-53.8	-67.8	-43.7	3.7
SANT	-33.2	-70.7	-23.1	1.5
SMAR	-29.8	-53.7	-20.1	17.2
SPED	18.5	-69.3	28.3	3.2
UNPM	20.9	-86.9	30.3	-15.8
UNPA	-51.6	-69.2	-41.5	2.6
VOIL	18.5	-72.3	29.2	-1.0

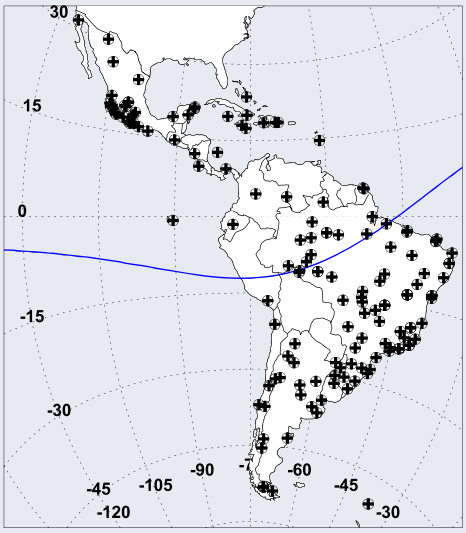

Note. Columns correspond to receiver station name, geographic position, and magnetic position (magnetic latitude ≡ mlat and magnetic longitude ≡ mlon). On the right, location map of GNSS receivers used to estimate the vTEC. The blue line on the map represents the magnetic equator in 2011.

daytime (Romero-Hernandez et al., 2018). In that study, the seasonal vTEC variability and different anomalies were discussed in order to characterize the ionosphere dynamics over this region. In light of enhancing the above discussion, this ionospheric study aims to analyze the nighttime electron density variations, particularly in the periods of 21:00, 00:00, and 03:00 LT, in the Northern and Southern hemispheres over the Latin American sector. It is based on the GNSS measurements obtained over 2 years, corresponding to two different phases of Solar Cycle 24: 2011 (the ascending phase) and 2014 (the maximum). This analysis examines the vTEC trend in relation to the solar flux and seasons, as well as its dependence on the receiver position. Thus, by studying the electron density variations at these periods, a fairly comprehensive point of view of the influence of those phenomena on the ionosphere over Latin America may be provided.

2. Observations and Methods

We employed data from a set of GNSS receivers distributed over Mexico, Central America, and South America, which are part of the following networks: National Seismological Service-Trans-boundary, Land and Atmosphere Long-term Observational and Collaborative Network (SSN-TLALOCNet → Mexico), Continuous Monitoring Network (COCONet → Central America), Brazilian Network for Continuous Monitoring of the GNSS Systems (RBMC), *Red Argentina de Monitoreo Satelital Continuo* (RAMSAC), and International GNSS Service (IGS → South America). Table 1 shows the list and geographical locations of the abovementioned GNSS receivers. The exact geographic locations are also indicated on the map on the right-hand side (see also Romero-Hernandez et al., 2018).

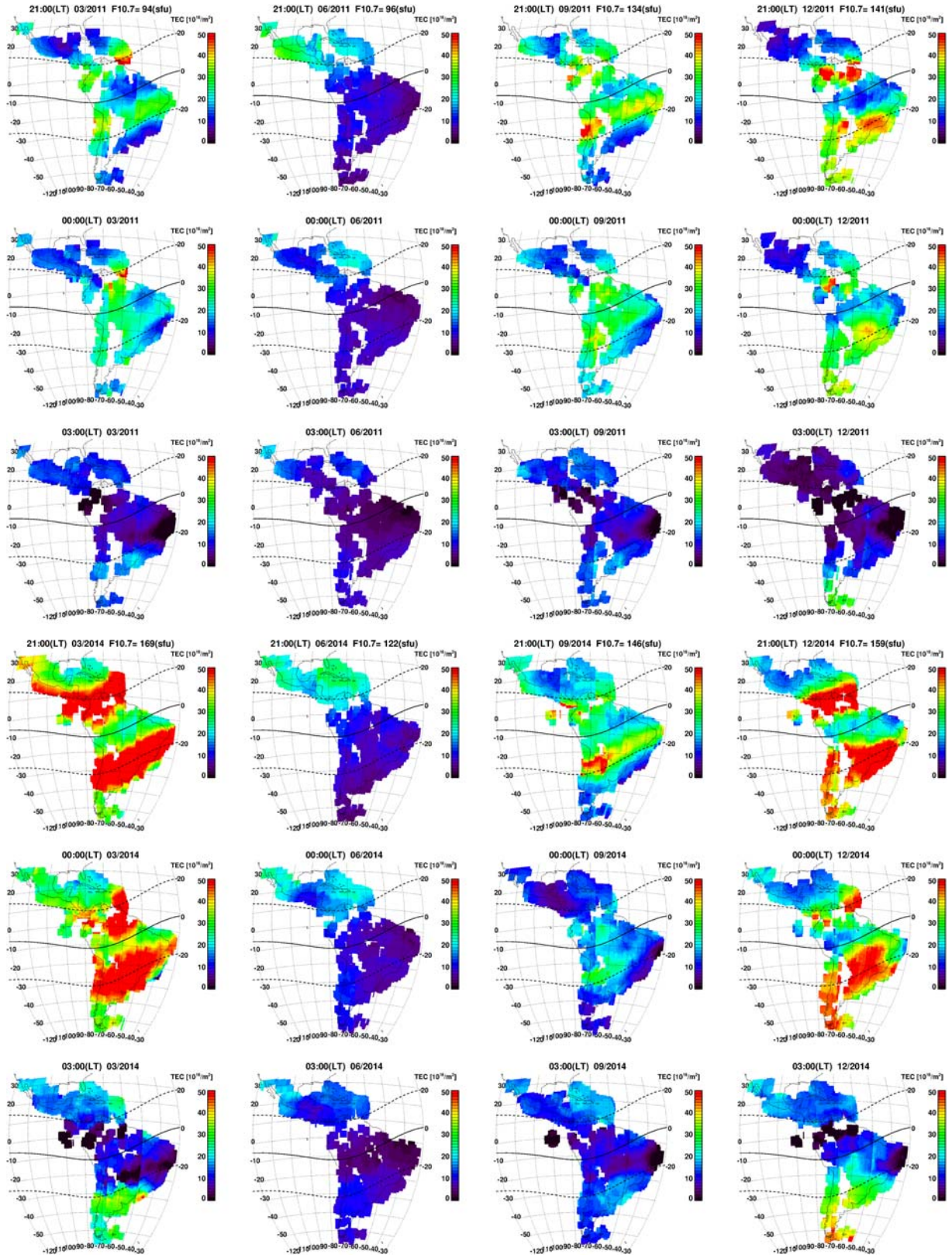

Figure 1. Monthly averaged TEC maps obtained at 21:00, 00:00, and 03:00 LT, corresponding to March, June, September, and December of 2011 (above) and 2014 (below). The solid black line represents the magnetic equator in 2011, and dashed lines correspond to magnetic latitudes at ±20°.

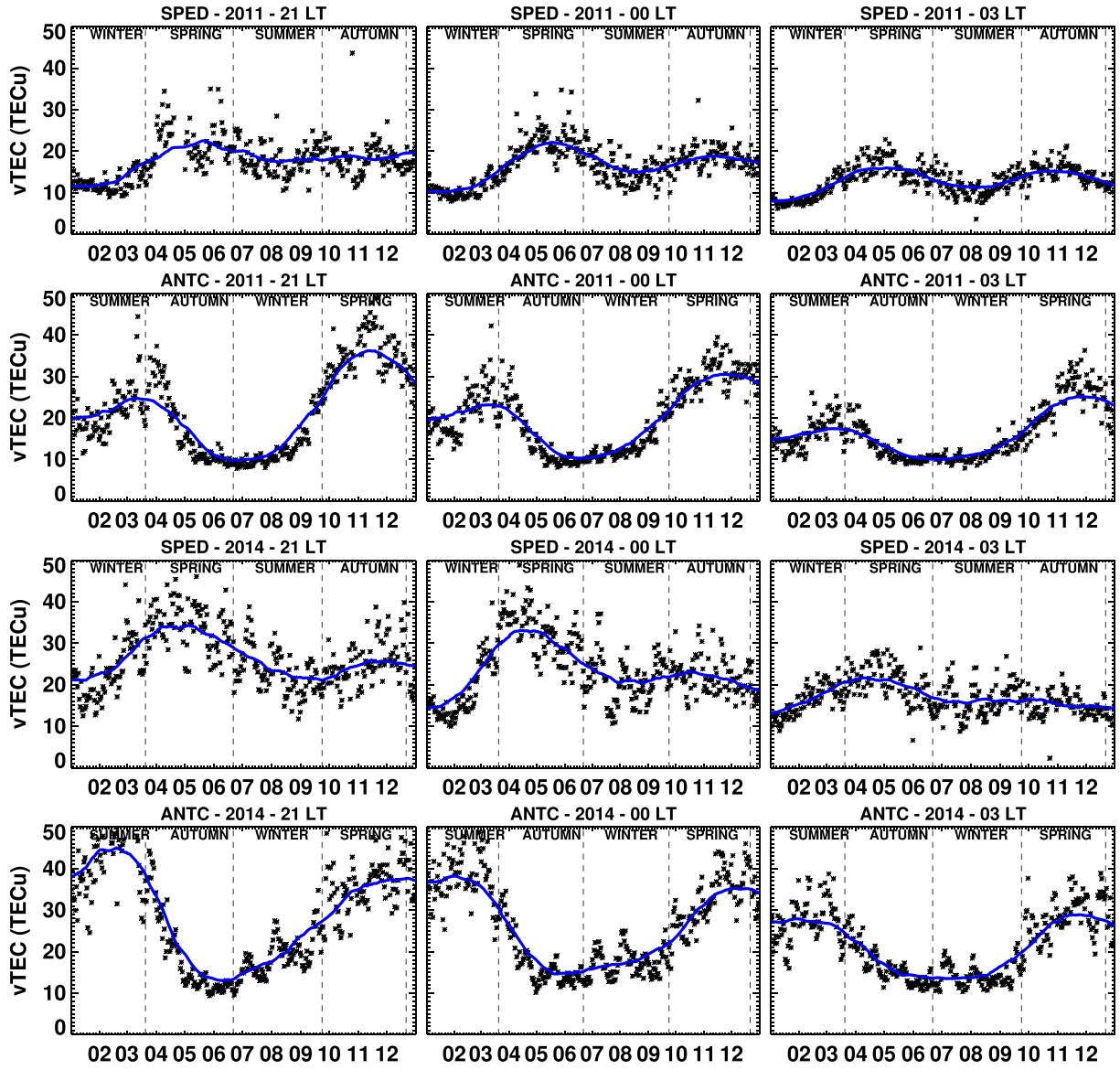

Figure 2. The vTEC variation curves at 21:00, 00:00, and 03:00 LT constructed during 2011 and 2014. These curves correspond to two GNSS receivers located in the Northern (SPED) and Southern (ANTC) Hemispheres. The blue solid lines represent the average vTEC trend at 21:00, 00:00, and 03:00 LT after removing the short-term variations. The black dashed lines mark equinoxes and soltices.

2.1. vTEC Variation Over Selected Receiver Stations

Two approximations are required to estimate TEC by using GNSS data. The first is based on the pseudoranges (pseudo-distances between the satellite and the receiver), calculated by mean a linear approximation: light velocity multiplied by the time difference between the emission and reception of the signal. The second uses phase differences between two signals (carrier phases). In this case, the TEC approximation was obtained using the methodology of the Space Weather Study and Monitoring Brazilian Program (*Estudo e Monitoramento Brasileiro de Clima Espacial* [Embrace]) at the *Instituto Nacional de Pesquisas Espaciais*, here referred to as TECMAP, with an estimate that is based on the approximation of Otsuka et al. (2002). This method uses both pseudoranges (P_1, P_2) and carrier phases (L_1, L_2) measurements to estimate the slant TEC. The vertical TEC (vTEC) is then obtained by multiplying the slant TEC by the ratio between the length of the ray path between altitudes of 250 and 450 km and the thickness of the ionosphere (slant factor) for the zenith path. To reduce the leveling errors, this method only considers those satellites with an elevation angle above 30°. The error in this approximation is less than 3 TECu (1 TECu = 10^{16} electrons/m^2) (Mannucci et al., 1998; Otsuka et al., 2002; Takahashi et al., 2016).

Table 2
Solar Flux Values for 2011 and 2014, Using the 81-Day Running Average of Daily Solar Radio Flux at 10.7 cm (F10.7A)

Year	Phase	Avg F10.7A (sfu)	Min F10.7A (sfu)	Month	Max F10.7A (sfu)	Month
2011	ascending phase	112.9 ± 19.4	87 ± 2.3	Jan, Jul	146 ± 2.6	Oct–Nov
2014	maximum	144.5 ±12	126 ± 0.9	Jul	163 ± 0.4	Jan

Note. The columns correspond to the following: year, phase of solar cycle, average F10.7A, minimum of F10.7A, month of occurrence, maximum of F10.7A, and month of occurrence.

TECMAP estimates vTEC with a time resolution of 10 min. Taking into account this resolution, an hourly average of vTEC at 21:00, 00:00, and 03:00 LT was estimated for representing the nighttime vTEC trend. This process was repeated for all GNSS receivers that were available in 2011 and 2014. Based on this approximation, both monthly averaged vTEC and vTEC variation curves (referred to as the nighttime average vTEC trend) were calculated. It is important to mention that for these approximations we are considering the vTEC values associated with geomagnetically quiet days only. For the present study, these days satisfy the following criteria: Dst > -30 nT, Σ Kp < 24 (Σ Kp $\equiv$ daily sum of values recorded by the eight magnetic observatories), and AE < 500.

The TEC maps in Figure 1 illustrate the resulting monthly averaged vTEC over Latin America. From left to right, the panels correspond to March, June, September, and December, representing solstitial and equinoctial months, and each row shows the spatial vTEC variation for a particular time. From the top to the bottom, each row corresponds to the following: 21:00 LT, 2011; 00:00 LT, 2011; 03:00 LT, 2011; 21:00 LT, 2014; 00:00 LT, 2014; and 03:00 LT, 2014. The solid line represents the magnetic equator, and the dashed lines correspond to ±20° magnetic latitudes. These maps reveal a seasonal vTEC variation, hemispheric differences, and some ionospheric anomalies, which will be analyzed and discussed in the following sections.

The nighttime average vTEC trend was constructed for the GNSS receivers listed in Table 1. An 81-day running average was applied in order to eliminate the short-term variations that are not considered. Figure 2 shows an example of a set of vTEC variation curves for 2011 (in the first two rows) and 2014 (in the bottom rows). These correspond to two GNSS receivers located in the northern (SPED [28° magnetic latitude (mlat)]) and southern (ANTC [−27° mlat]) magnetic hemispheres, respectively. The asterisks represent the vTEC for each day at 21:00, 00:00, and 03:00 LT, and the solid line represents the average vTEC trend. The seasons are also indicated in this figure, and the dotted lines represent the equinoxes and solstices. Note that in comparison to daytime, the vTEC scale of these and consecutive plots has been reduced to highlight the nighttime trend.

2.2. vTEC Variation With Respect to the Solar Activity and Seasonality

The effects of solar activity on the nighttime vTEC variation are analyzed in terms of solar radio flux at 10.7 cm (F10.7). We adopted the P solar activity factor $\rightarrow P = (F10.7 + F10.7A)/2$ as a solar proxy to represent the EUV variability (Chen et al., 2012; Liu et al., 2006). In this approximation, F10.7A is referred to as the 81-day running average of daily F10.7. The general properties of the two years based on solar radio flux variation are presented in Table 2. From left to right, the columns correspond to year, phase of the solar cycle, average F10.7, the minimum of F10.7A with their respective month of occurrence, and the maximum of F10.7A with their respective month of occurrence.

To evaluate the influence of solar radiation on the average vTEC trend, the relation between the P solar activity factor and the day-to-day vTEC was analyzed. An average vTEC variation curve in each hemisphere was obtained by using a set of GNSS receivers located at different latitudes in a narrow longitudinal band: SPED, PUIN, IQQE, LRBR, ALUM, and SANT (with their coordinates listed in Table 1). In this way, three average vTEC curves were calculated. The first one is the average of all GNSS receivers, named total average vTEC curve. The second one corresponds to the northern vTEC variation, calculated using only receivers in the Northern hemisphere (SPED [28° mlat], PUIN [13° mlat], and LRBR [0.01° mlat]). Finally, the third one represents the southern vTEC variation, which is calculated by averaging the receivers in the Southern Hemisphere (IQQE [−11° mlat], ALUM [−17° mlat], and SANT [−23° mlat]). Figure 3 shows the correlation between the P factor and the three average vTEC curves constructed for 2011 (left panels) and 2014 (right panels), indicating in each case the Pearson's correlation coefficient (R). The error bars correspond to the standard deviation of averaged vTEC values.

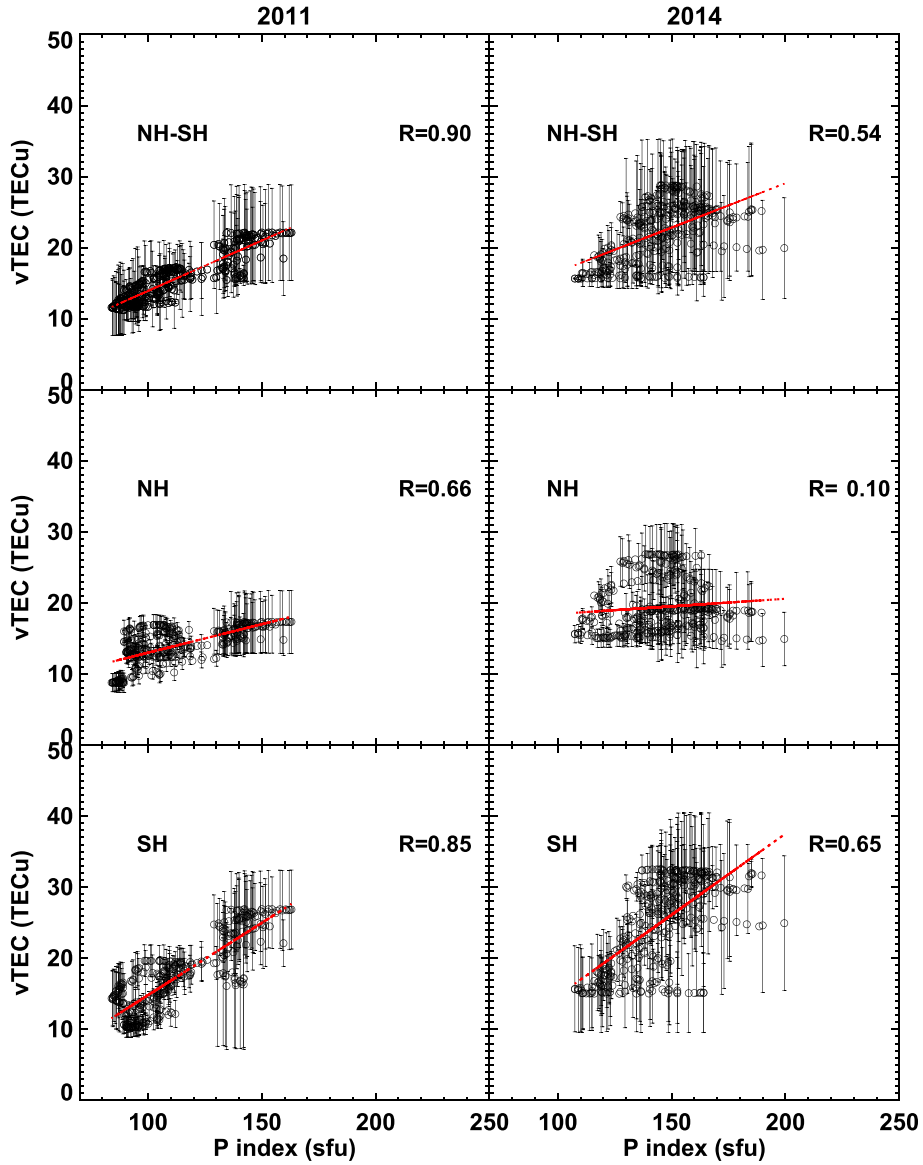

Figure 3. Relation between the *P* solar activity factor and the average vTEC curves in the NH and SH during 2011 and 2014. Each case corresponds to the following: NH-SH → the average of all GNSS receivers (total average vTEC curve); NH → the northern vTEC variation (NH average vTEC curve); and SH → the southern vTEC variation (SH average vTEC curve). The error bars correspond to the standard deviation of averaged vTEC values.

3. Results and Discussion

The discussion of nighttime vTEC variation focuses on hemispheric differences associated with the solar activity and seasonal variation. Henceforth, we refer to the Northern and Southern Hemispheres as NH and SH, respectively.

3.1. vTEC Variation at Two Different Phases of the Solar Cycle

During the nighttime, the ionization ratio becomes lower compared to daytime due to the absence of solar radiation. Thus, the electron density is expected to be smaller. Nonetheless, as Figures 1 and 2 reveal, there are notable differences of vTEC between the years 2011 (ascending phase) and 2014 (maximum). From Figure 1, comparing both years, it is noted that vTEC values were higher in 2014 than in 2011, which agrees with the increment of solar flux associated with the solar maximum. Moreover, significant differences of vTEC can be distinguished during these years, identifying a maximum level of ionization qualitatively during December and a minimum level of ionization in June. According to Table 2, this vTEC

minimum occurred near to the minimum of solar radio flux (July), which is congruent and partially explains this fall, although, in general, the electron density in the June solstice is expected to be lower than in December solstice because the interhemisphere thermospheric circulation promotes a smaller $[O]/[N_2]$ ratio. The asymmetric heating between winter and summer hemispheres drives an interhemispheric flow, that is, a plasma flux from the summer-to-winter region, which affects the neutral composition and the recombination processes (Fuller-Rowell, 1998; Rishbeth & Mendillo, 2001).

In the same way, minimum and maximums are identified in the vTEC variation curves presented in Figure 2. Here, vTEC variation is mainly characterized by two crests associated with periods of maximum ionization at night, except for SPED-2014 that shows only one crest. Such crests are usually associated with equinoxes; however, in this case, they do not correspond to March and September equinoxes. Taking as a reference the black dashed lines in this figure, representing the equinoxes and solstices, a temporal dephasing is noted in these crests. They occurred at different times in each hemisphere since they were observed in April–May and October–November in the northern receiver, while in the southern receiver, they occurred through March and November. For simplicity henceforth, we refer to them as March and November crests, respectively.

According to Table 2, the minimum values of the average vTEC variation registered in June–July coincide with the minimum F10.7A, while the maximum values were better correlated with the maximum F10.7A in the southern receiver (ANTC [−27° mlat]) than in the northern receiver (SPED [28° mlat]). This preliminary result also makes evident the disparity of the vTEC trend between the two hemispheres (hemispheric asymmetries). In addition, in both receivers, a higher vTEC was registered in 2014 when compared to 2011. It was expected because of the increment of solar radiation flux during the maximum of the solar cycle.

Another substantial effect is the reduction of vTEC intensity according to the night progresses. This effect can be better visualized in Figure 1, which is congruent with the diminishing photoionization. By considering UNPM (30° mlat) and ANTC (−27° mlat) receivers in the NH and SH, respectively, as a sample to show the diminishing rate of vTEC from 21:00 to 03:00 AM LT, we found out that in 2011 there was a vTEC diminishing of 28.2% in the NH and 27.3% in the SH, while for 2014 the vTEC diminishing was 19.7% in the NH and 29.4% in the SH. The photoionization process, however, is not dominant in the configuration of the nighttime vTEC trend.

Analyzing the relation between the P solar activity factor and the vTEC variation, good correlations (>0.5) were found in 2011 (see Figure 3). For example, the total average vTEC curve showed the highest correlation ($R = 0.9$), while the NH average vTEC curve presented the lowest (0.6). It means that during this year, the vTEC trend was more strongly influenced by the solar flux variation. For 2014, poor correlations were obtained, however, suggesting a low interdependence between vTEC and the solar flux. By considering vTEC variation in the NH (middle panels), the analysis shows the lowest correlation ($R = 0.1$), which indicates a nonlinear dependence between TEC variation and the solar flux. Such fact suggests, as occurs in the daytime, that in high solar activity another mechanism plays a role in the nighttime ionosphere dynamics. This could be attributed to the thermospheric wind and PRE. Additionally, the differences observed in Figure 3 between the correlations obtained for the NH and SH reveal a strong hemispheric asymmetry. Comparing the error bars in both hemispheres, a big latitudinal gradient of vTEC may be inferred, especially in the SH, emphasizing hemispheric asymmetries at night. These asymmetries will be discussed in section 3.3.

Another important feature identified in the maps of Figure 1 is the EIA. Electron density enhancements around ±15° magnetic latitude (dashed lines) are visualized during March, September, and December, which also exhibit notable differences between the two years. As mentioned in section 1, the nighttime EIA results from the PRE. The influence of PRE is expected to be significant until midnight local time, especially during severe magnetic storm periods (e.g., Lyon & Thomas, 1963). Nonetheless, studies such as McDonald et al. (2008) and Yizengaw et al. (2009) have reported postmidnight EIA signatures during magnetically quiet periods. In this regard, the differences between EIA at 00:00 and 03:00 LT in Figure 1 suggest that in these periods, the magnitude of PRE rapidly diminished after midnight since the EIA became imperceptible at 03:00 LT. Comparing the vTEC maps in 2014 and 2011, we also inferred that the PRE was stronger in 2014, when the vTEC level was higher.

3.2. Overall Seasonal vTEC Variation at Night

Although the vTEC level at night is much lower than in daytime, the spatial and temporal variations shown in Figure 1 reveal significant differences between equinoxes and solstices. The vTEC variation curves

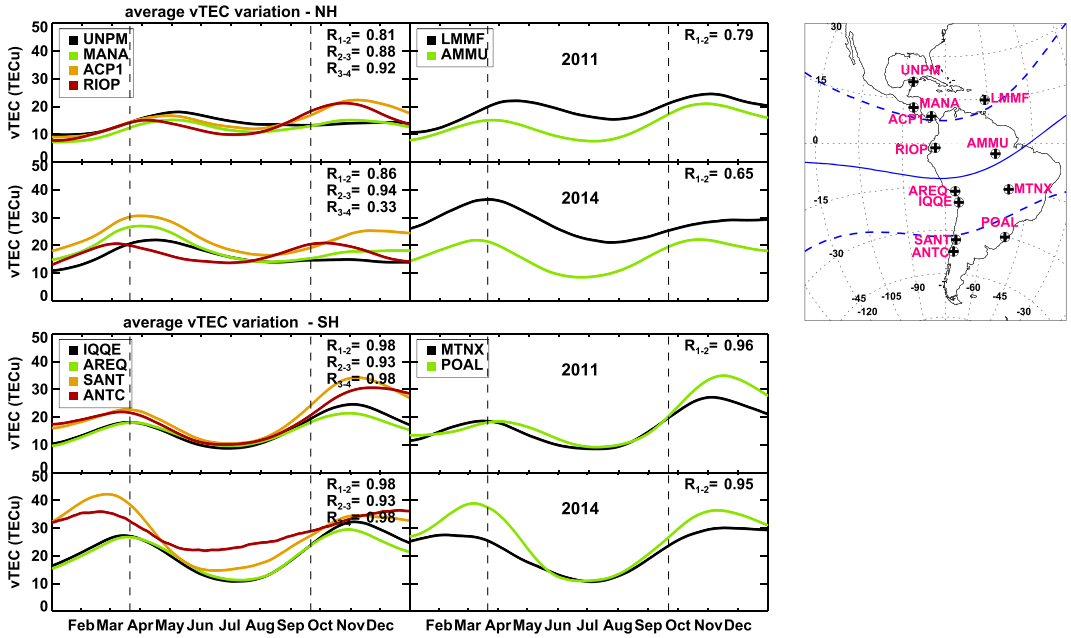

Figure 4. Comparison of the average vTEC variation representing nighttime trend during 2011 and 2014, for a set of GNSS receivers distributed at different latitudes. The *R* value is the linear correlation between GNSS receivers enumerated in the same order as are listed in the label. Geographic and magnetic coordinates of these receivers can be consulted in Table 1.

presented in Figure 2 emphasize this seasonal behavior, exhibiting some anomalies characteristic of the vTEC trend.

By considering the daytime vTEC trend, this seasonal behavior at night should be a residual effect from that observed in the daytime (see Figure 3 of Romero-Hernandez et al., 2018). It means that the seasonal trend of nighttime vTEC could be similar to that of the daytime, as seems to be anticipated from Figure 2. To analyze this scenario, a set of GNSS receivers at different latitudes in a narrow longitudinal band was selected: UNPM, MANA, ACP1, RIOP, AREQ, IQQE, SANT, and ANTC (geographic and geomagnetic coordinates can be consulted in Table 1). In a similar way to Figure 2, the average vTEC variation curves were constructed for each GNSS receiver from averaging the vTEC variation curves of the three hours analyzed (21:00, 00:00, and 03:00 LT). Figure 4 shows the comparison of average-vTEC variation curves during 2011 and 2014, and the map on the right-hand side shows the location of the GNSS receivers involved. This comparison was divided into four groups depending on the longitudinal band and hemisphere where the receivers are located. The first and second groups correspond to those receivers within a longitudinal band from −90–75° in the NH (UNPM [30° mlat], MANA [21° mlat], ACP1 [20° mlat], and RIOP (8° mlat]) and SH (AREQ [−6° mlat], IQQE [−11° mlat], SANT [−23° mlat], and ANTC [−27° mlat]). The third and fourth groups (in the panels on the right side) correspond to receivers into a longitudinal sector from −60° to −45° located in the NH (LMMF [24° mlat] and AMMU [6° mlat]) and SH (MTNX [−5° mlat] and POAL [−21° mlat]). The *R* values correspond to Pearson's correlation coefficients between the GNSS receivers enumerated in the same order as they appear on the labels. According to these plots, all the receivers exhibiting a similar trend as that one in the daytime showed a regular signature of this semiannual anomaly at night, except for UNPM (30° mlat) and MANA (21° mlat) where the November crest was not present. The configuration of the semiannual anomaly was different, however, depending on the latitude and year. All receivers showed ionization crests at different times; hence, the correlation coefficients associated with these average vTEC variation curves were lower than those in the daytime. The lowest correlations were registered in 2014, and they were associated with receivers in the NH, which suggest a large latitudinal variability of the vTEC trend.

Another important aspect to highlight in these plots is that the latitudinal effect of vTEC observed in the daytime, in which vTEC becomes lower with the increment of latitude, was absent after midnight. The GNSS receivers located at midlatitudes registered similar values of vTEC as those receivers at low latitudes (in particular for this set were SANT, LMMF, and POAL), which may be related to change in the thermo-

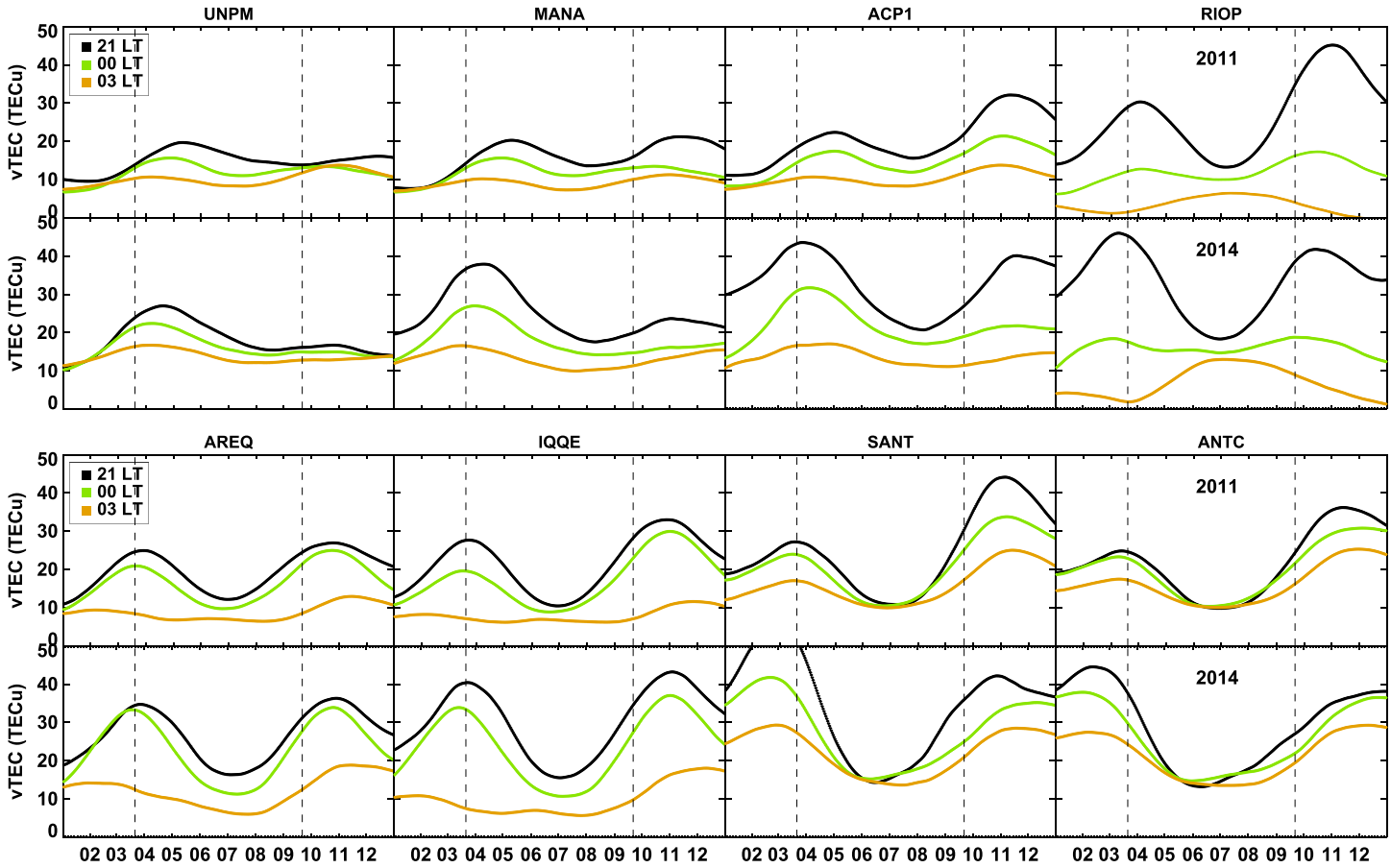

Figure 5. Comparison of the vTEC variation curves of the GNSS receivers of Figure 4, obtained at 21:00 (black line), 00:00 (green line), and 03:00 (orange line) LT in 2011 and 2014. The dashed lines indicate equinoxes.

sphere processes and wind system in the lower and middle latitudes during nighttime. Jonah et al. (2015) and Jee et al. (2005) using observation and model, respectively, studied the sensitive of geomagnetically quiet period to the atmosphere and ionosphere parameters including neutral wind and pointed out that the meridional component of the neutral wind during both day and night significantly affect TEC variation.

To analyze the evolution of the seasonal vTEC trend with the night progresses, we compared the three variation curves of some receivers used in Figure 4, which were obtained at 21:00, 00:00, and 03:00 LT. This comparison is showed in Figure 5, in which each hour has been indicated with a different color: black → 21:00 hr, green → 00:00 hr, and orange → 03:00 hr. As was expected, an attenuation of the seasonal trend according to the night progresses was observed, which is congruent with the reduction of vTEC. Such attenuation becomes more evident as we move toward equatorial regions; hence, the receivers ACP1 (19° mlat), RIOP (8° mlat), AREQ (−6° mlat), and IQQE (−11° mlat), located around ±20°, showed a very weak seasonal trend at 03:00 a.m. LT. Moreover, the vTEC trend of the RIOP receiver exhibited a high variability with the night progresses. Its vTEC trend at 03:00 AM was very distinct from the other receivers, presenting a predominant maximum during June–July in the two years.

From Figure 5, we note that in 2014 the semiannual anomaly was absent in the receivers at midatitudes (UNPM and MANA). As was mentioned before, these receivers exhibited an asymmetric seasonal trend, with only one ionization crest in March–April.

Based on the above analysis, some other anomalies are discussed in the next subsections to complement the description of the seasonal vTEC behavior.

3.2.1. Annual Anomaly

From Figure 2, we can observe that ANTC (−27° mlat) receiver shows a significant difference between the vTEC values during the December and June solstices ($\Delta TEC_{DJ} \equiv \Delta TEC_{December} - \Delta TEC_{June}$), suggesting the

presence of the annual anomaly in the SH. By using the average vTEC variation such a difference was quantified, having that for ANTC-2011 $\Delta TEC_{DJ} = 14.8 \pm 4.9$, while for ANTC-2014 $\Delta TEC_{DJ} = 14.4 \pm 8.1$. On the other hand, by analyzing the maps in Figure 1, we found that the signature of the annual anomaly (by taking the NH and SH together, *NmF2* is higher around December than around June; Zhao et al., 2008) diminished with night progresses. This anomaly became imperceptible at 03:00 a.m. LT. To corroborate this fact, the vTEC differences (ΔTEC_{DJ}) between December and June were estimated using all the average vTEC values calculated over Latin America. According to the hour, these vTEC differences were as follows: to 21:00 LT $\rightarrow \Delta TEC_{DJ}$-2011 = 4.9, ΔTEC_{DJ}-2014 = 17.1; to 00:00 LT $\rightarrow \Delta TEC_{DJ}$-2011 = 7.3, ΔTEC_{DJ}-2014 = 13.1; to 03:00 LT $\rightarrow \Delta TEC_{DJ}$-2011 = 2.3, and ΔTEC_{DJ}-2014 = 4.6. By comparing such differences, we can infer that the annual nighttime anomaly in 2014 was stronger than in 2011. It presented a decrement with time, especially visible in 2014.

Another interesting aspect in Figure 2 is the presence of equinoctial asymmetry. As with the daytime, we found out that one out of two crests was predominant in the vTEC trend of each year: a main maximum of ionization was present in each year. For instance, ANTC-2011 shows a predominant November crest, while for ANTC-2014 the March crest was larger. This aspect may be mainly related to the solar flux, since analyzing the months where F10.7A was maximum, they were close to these predominant crests (see Table 2). For ANTC-2014, however, such equinoctial asymmetry became imperceptible at 03:00 AM LT, which indicates a stronger vTEC variability at night. In the case of the SPED receiver, such asymmetry was more evident in 2014, when the November crest disappeared.

3.2.2. Nighttime Winter Anomaly

A weak NWA (higher N_mF_2 in winter than in summer) was observed in Figure 1: the vTEC values in both summer and winter were comparable in the NH. To quantify this fact, a monthly vTEC average for January and June, representing winter and summer, was calculated to determine the vTEC differences between both winter and summer (ΔTEC_{W-S}). Thus, these differences were as follows: at 21:00 LT $\rightarrow \Delta TEC_{W-S}$-2011 = −13.3, ΔTEC_{W-S}-2014 = −4.2; to 00:00 LT $\rightarrow \Delta TEC_{W-S}$-2011 = −6.1, ΔTEC_{W-S}-2014 = −2.4; and to 03:00 LT $\rightarrow \Delta TEC_{W-S}$ − 2011=-3.2, ΔTEC_{W-S}-2014 = −3.0. These negative differences indicate that the vTEC values in summer were greater than those in winter, suggesting a possible absence of NWA. Because these differences were estimated using all GNSS receivers in the NH, distinct seasonal behaviors may be mixed in this result. That is why we cannot assume a complete absence of this anomaly.

By analyzing the individual behavior of GNSS receivers in the NH (as in Figures 4 and 5), we also found a weak signature of the NWA, which had similar values of vTEC during January and June of the two years. Analogous results were found when Balan et al. (2000) analyzed electron density data from MU radar in Japan (34° N and 136.1° E) during Solar Cycle 22. They reported that at night the winter anomaly disappears. As they indicated, one explanation for this phenomenon is related to the meridional winds. From the chemical composition in the *F* layer, nitrogen molecule is more abundant in the June solstice than in the December solstice (low $[O]/[N_2]$ ratio), and this contributes to ionization reduction in June, which causes a strong daytime winter anomaly. At night, however, the presence of strong equatorward winds may produce an increment in the electron density during June. In the next section, we will explore the neutral winds profile to support this explanation. More recently, Sai Gowtam and Tulasi Ram (2017), by using FORMOSAT-3/COSMIC radio occultation, concluded that the midlatitude NWA did not occurred during the ascending phase of Solar Cycle 24 (2011 and 2012). From our analysis, this conclusion may be extended to the maximum of Solar Cycle 24.

Results from Jakowski et al. (2015) indicated that the NWA is associated with periods of low solar activity (F10.7 around 80–120 sfu). They explained that the low ionization level at low solar activity conditions provokes the interhemispheric plasma fluxes (interhemispheric circulation) generate intense downward fluxes, increasing the electron density in winter. In our case, for 2011, the solar radio flux was around 80–140 sfu; however, the NWA was almost absent. This fact suggests that for this period such interhemispheric circulation was feeble in increasing the electron density.

3.2.3. The EIA

By analyzing the EIA evolution over the two years (see the TEC maps provided in the supporting information), we found that it presented a seasonal behavior similar to the vTEC trend. It means the EIA signature was more robust during the months associated with the ionization crests, that is, April and November for 2011 and March and November for 2014. The EIA signature was absent from June to August, which

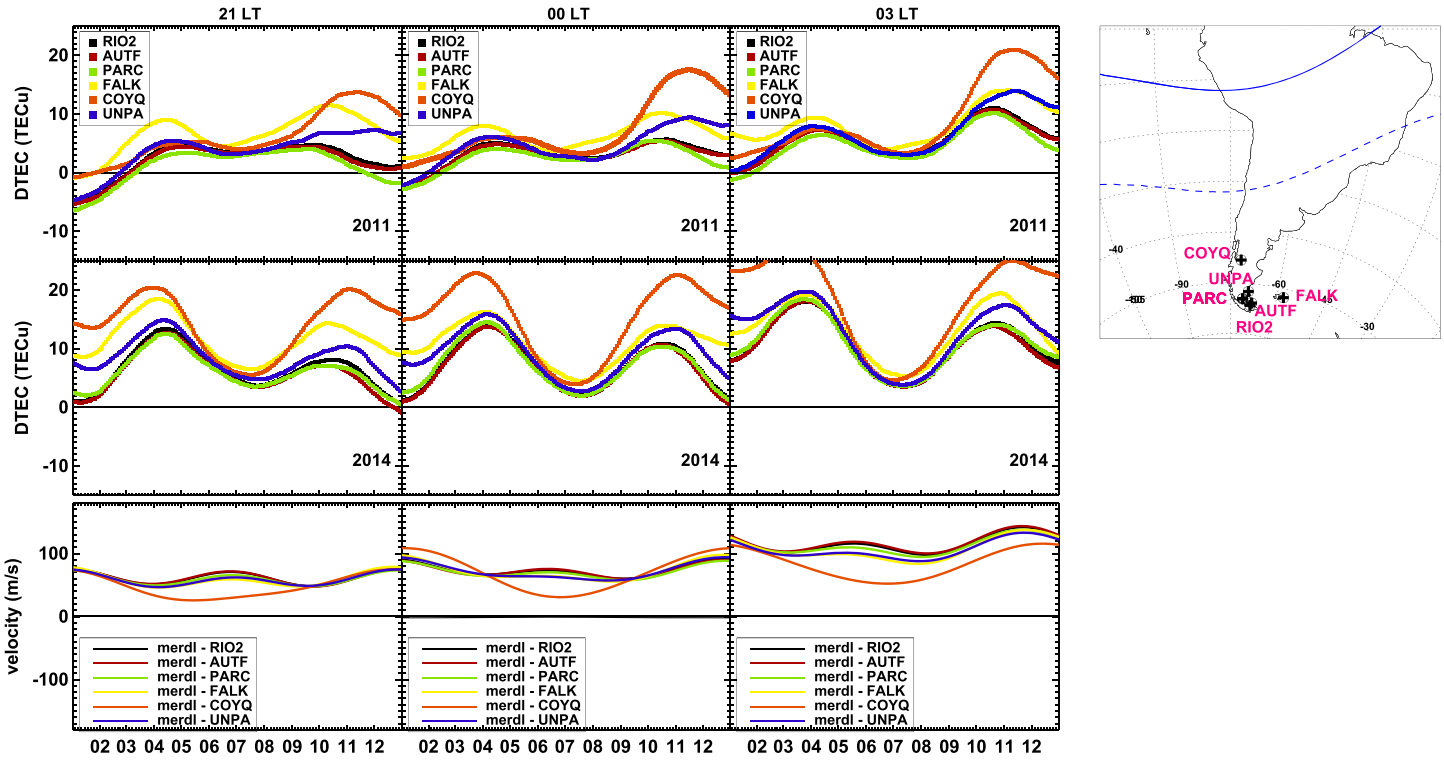

Figure 6. Day-night vTEC differences (DTEC) estimated for some GNSS receivers located in the southern Argentina and Chile (see the right-hand side of the map). Here, daytime vTEC corresponds to 12:00 LT, while nighttime vTEC refers to 21:00, 00:00, and 03:00 LT. In addition, their respective DTEC has been plotted by columns for the two years. The bottom panels show the meridional wind component of the velocity approximated by using the HWM-2014 model.

coincides with the period of minimum vTEC. Particularly for these 3 months, especially June, the hemispheric disparity became more evident. After calculate the average vTEC of each hemisphere, we found significant differences (for 2011: vTEC-NH = 21.8 ± 3.8 TECu, vTEC-SH = 10.4 ± 4.3 TECu; for 2014: vTEC-NH = 22.3 ± 2.1 TECu, vTEC-SH = 10.1 ± 4.0 TECu). The highest vTEC values were registered in the NH in the two years, coinciding with the summer hemisphere. Such hemispheric differences can also be visualized in the vTEC trend since, during June, the NH presented higher values of vTEC than the SH (see Figures 4 and 5). Contrary to the daytime observations, in which the highest vTEC values were extended to receivers in the SH (see Figure 2 in Romero-Hernandez et al., 2018), this suggests a small interhemisphere thermospheric circulation at night. In other words, if the summer-to-winter meridional wind circulation is not enough to generate a plasma flux, then the electron density tends to be higher in the summer hemisphere than in the winter hemisphere. As was suggested before, such an effect could also explain the weak NWA.

We observed that in December of 2014 the southern part of the EIA seemed to be extended to higher latitudes. Such intensification could be related to the MSNA, which is discussed in the next subsection.

3.2.4. Midlatitude Summer Nighttime Anomaly

An intensification of the vTEC values in the southernmost part of the SH was observed during December 2011 and December 2014, which seems to be associated with the presence of MSNA (see Figure 1). From monthly averaged vTEC maps, this effect was identified in the GNSS receivers at midlatitudes (under −40°). To corroborate this fact, a day-night vTEC comparison was performed by using some receivers located in southern Argentina and Chile (RIO2 [−43° mla], AUTF [−44° mlat], PARC [−43° mlat], FALK [−41° mlat], COYQ [−35° mlat], and UNPA [−42° mlat]). Figure 6 shows the day-to-day vTEC differences (DTEC) between day → 12:00 and night → 21:00, 00:00, and 03:00 LT, in the two years. Here, a positive DTEC indicates a large vTEC during the daytime, while a negative DTEC indicates a large vTEC in the nighttime. According to these plots, negative values of DTEC occurred mainly during January and February of 2011, which coincide with summer in the SH. The maximum negative DTEC was around −5 TECu and was registered by the PARC, AUTF, RIO2, and UNPA, receivers located under −40° mlat, while for COYQ and FALK receivers, the vTEC values were similar in the day and at nighttime. Observing Figure 6, we can see that although this negative DTEC was not so significant when compared to positive DTEC, it marks a period of

anomalous vTEC behavior present only in 2011. Thus, this result confirms the presence of MSNA during the ascending phase of Solar Cycle 24 (moderate solar activity). As we mentioned in section 1, this anomaly has also been reported during December. In this case, three out of six receivers exhibited a low DTEC during December 2011, which may be considered as a weak MSNA (the vTEC values were comparable during the day and night).

Some authors have explained the MSNA in terms of the meridional circulation of neutral wind at night. They suggest that the electron density enhancement results from the plasma displacement caused by equatorward neutral winds (Lin et al., 2010; Thampi et al., 2011). To explore this argument, we included in our analysis the meridional neutral wind component approximated by using the newest version of the Horizontal Wind Model of 2014 (HWM-14) (Drob et al., 2015). The bottom panels in Figure 6 show the meridional wind component (labeled as "merdl") estimated for each receiver location. It is important to mention that this model has some limitations such as no solar activity dependence, which means that no differences between the wind trend in different years can be identified. For that reason, only one trend is reported for the two years. Based on the HWM-14 approximations, we found that on average the meridional wind was moving to the north (equatorward wind) presenting the higher velocities during January, June, and December. Thus, the presence of equatorward winds in January could help to explain the formation of MSNA. In addition, during January, the EIA exhibited one crest in the SH, which suggests downward plasma fluxes associated with the fountain effect. The interaction of these plasma fluxes with the equatorward winds could help to explain such vTEC enhancement. For instance, Qian et al. (2016), modeling the effect of the EIA on the interhemispheric circulation during solstices, found that in the summer hemisphere ion drag because the EIA suppresses the meridional winds, which may increase the $[O]/[N_2]$ ratio at midlatitudes. Furthermore, during the daytime, meridional winds in the SH were moving to the south, then such an interaction did not occur (see Figure 6 in Romero-Hernandez et al., 2018).

Additionally, we noted that although the velocity of meridional neutral winds was incrementing with the night progresses, the intensity of the MSNA diminished and was imperceptible at 03:00 a.m. It suggests that the reduction of the electron density after midnight interfers with the MSNA formation, such as with the other anomalies. This fact also is congruent with the absence of the MSNA in June since during this month the values of TEC, in general, were very low (<15 TECu). Nonetheless, further observations are needed to corroborate this fact.

From Figure 1, we also note vTEC enhancements in December 2014. Based on the DTEC, we can see that three out of six receivers showed DTEC values close to 0 TECu (see middle panels in Figure 6). It suggests again that the nighttime vTEC values were comparable to those in the daytime, which could mean a very weak MSNA. We cannot infer much about interhemispheric circulation, however, to explain the absence of the MSNA in 2014 because of HMW-14 limitations.

3.3. Hemispheric Dependence of Seasonal vTEC Variation

From previous sections, we have pointed out that the nighttime vTEC trend had a distinct response in each hemisphere. The seasonal vTEC variability, anticipated from Figure 1, presents a different behavior according to the receiver position and hour. As per the qualitative results of Figure 2, each hemisphere showed a distinct vTEC trend, with the southern receiver (ANTC) exhibiting a seasonal trend more similar to that in the daytime. Furthermore, by analyzing the seasonal trend at different latitudes in Figure 5, a larger variability is perceived in comparison to the daytime, especially in the NH (see Figures 4 and 5 in Romero-Hernandez et al., 2018). Receivers above 20° mlat (UNPM and MANA) showed an asymmetric seasonal trend without the November ionization crest.

In Figure 5, we can also observe that receivers at equatorial and low latitudes presented a rapid evolution with the night progresses. Receivers such as RIOP (8° mlat), ACP1 (20° mlat), AREQ (−6° mlat), IQQE (−11° mlat), AMMU (6° mlat), and MTNX (−5° mlat) showed a distinct seasonal trend for each hour, which became insignificant at 03:00 a.m. LT. Such a feature was observed during both years, that is, in moderate and high solar activity, suggesting that was generated by thermosphere processes.

It is well known that the dynamical upwelling and downwelling are the primary drivers for composition change ($[O]/[N_2]$ ratio) (Balan et al., 2000; Foster & Jakowski, 1988; McDonald et al., 2008; Medeiros et al., 1997; Qian et al., 2016). In general, the electrons and ions distributions are strongly influenced by the neutral winds. The plasma moving along the geomagnetic field lines may be forced to go upward

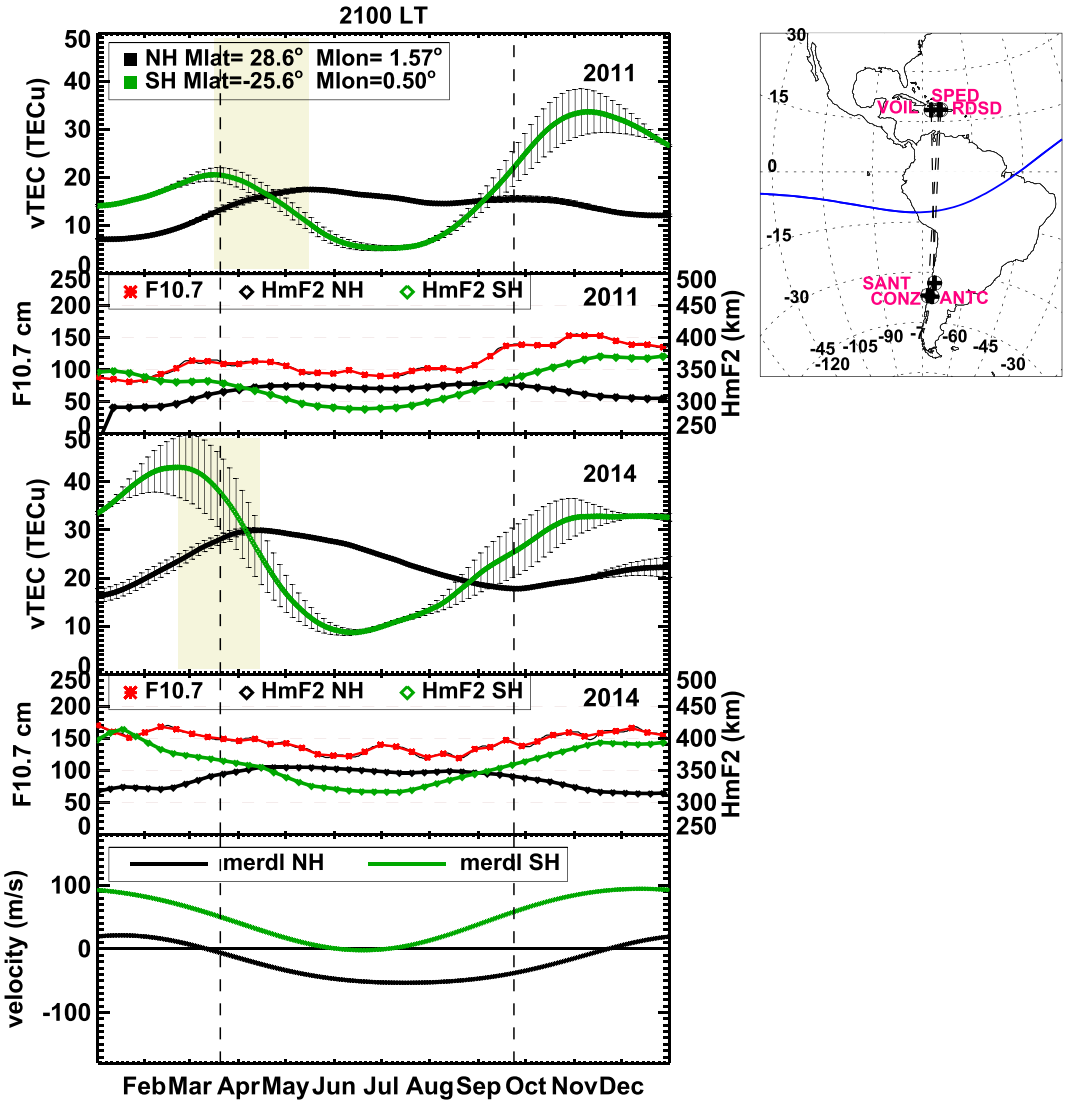

Figure 7. Comparison between the average vTEC variation curves at conjugate points, the solar radio flux F10.7A, and the H_mF_2. From top to bottom, the panels correspond to the following: the average vTEC variation in the NH (green line) and SH (black line), at 21:00 LT in 2011; the F10.7A (red line) and the h_mF_2 in the NH (green line) and SH (black line), at 21:00 LT in 2011; the average vTEC variation in the NH (green line) and SH (black line), at 21:00 LT in 2014; the F10.7A (red line) and the h_mF_2 in the NH (green line) and SH (black line) in 2014; and the meridional wind velocity in the NH (green line) and SH (black line) at 21:00 LT, approximated by the HMW-14 model. The map on the right-hand side indicates the position of the GNSS receiver used to estimate this average vTEC variation. Yellow bars indicate the time difference between the ionization crests of each hemisphere. Note the vTEC variation curves show the error bars associated with the standard deviation between the GNSS receivers used to construct the average vTEC variation.

or downward depending on the wind direction, changing the height of the density peak of the F_2 layer (h_mF_2), which at the same time affects the recombination processes and the electron density. Particularly, the nighttime ionosphere is strongly affected by these dynamic processes (Chen et al., 2008). In this sense, we performed an analysis to examine the role of neutral winds in the nighttime seasonal vTEC trend in both hemispheres.

Six GNSS receivers (RDSD [28° mlat], SPED [28° mlat], and VOIL [27° mlat] in the NH, as well as CONZ [−27° mlat], ANTC [−27° mlat], and SANT [−23° mlat] in the SH) close to conjugate points were selected according to their magnetic latitude and longitude (Mlat, Mlon) to construct an average vTEC variation curve for each hemisphere. Figure 7 examines the effect of both the solar flux and the meridional winds over the average vTEC variation at 21:00 LT. The different panels correspond to the following: the average vTEC variation in the NH (green line) and SH (black line) during 2011; the F10.7A (red line) and the h_mF_2 in the

Table 3
Comparison of the vTEC and the Average Height of the Density Peak of the F_2 Layer (h_mF_2) During Equinoctial and Solstitial Months Corresponding to March–April, June–July, October–November, and December of 2011 and 2014

	March–April		June–July		October–November		December	
Year	vTEC (TECu)	h_mF_2 (km)	vTEC (TECu)	h_mF_2 (km)	vTEC (TECu)	h_mF_2 (km)	vTEC (TECu)	h_mF_2 (km)
2011-NH 21 hr	11.9 ± 1.3	318.1 ± 6.4	13.0 ± 0.5	321.4 ± 1.0	12.0 ± 0.7	314.7 ± 5.7	10.6 ± 0.04	305.3 ± 0.1
2011-NH 00 hr	12.3 ± 2.6	304.8 ± 3.9	13.7 ± 1.8	311.3 ± 1.4	12.9 ± 0.5	294.4 ± 5.0	12.8 ± 0.1	289.8 ± 1.5
2011-NH 03 hr	10.7 ± 1.8	295.7 ± 5.8	9.2 ± 1.3	307.3 ± 0.4	11.4 ± 0.5	297.2 ± 2.7	9.1 ± 0.4	292.2 ± 0.3
2011-SH 21 hr	16.4 ± 1.4	322.1 ± 4.1	8.2 ± 0.3	291.8 ± 3.4	24.0 ± 1.6	360.8 ± 9.1	23.2 ± 0.6	369.6 ± 1.6
2011-SH 00 hr	16.0 ± 2.3	303.6 ± 1.9	6.0 ± 0.6	292.7 ± 1.0	25.0 ± 1.8	327.2 ± 7.8	24.8 ± 0.5	333.8 ± 1.4
2011-SH 03 hr	11.0 ± 1.3	284.9 ± 5.6	5.3 ± 0.3	278.9 ± 0.7	18.0 ± 2.0	307.5 ± 6.4	18.5 ± 0.5	321.6 ± 0.5
2014-NH 21 hr	24.7 ± 1.0	347.5 ± 7.1	22.0 ± 1.3	348.7 ± 2.2	19.7 ± 0.6	324.4 ± 7.7	20.0 ± 0.1	314.2 ± 0.4
2014-NH 00 hr	25.7 ± 2.9	317.7 ± 7.1	20.0 ± 2.5	324.4 ± 1.4	17.6 ± 0.6	299.1 ± 5.3	15.5 ± 0.4	294.6 ± 1.5
2014-NH 03 hr	18.5 ± 1.3	326.0 ± 5.2	13.5 ± 1.2	326.1 ± 2.1	12.5 ± 0.9	308.6 ± 3.9	10.3 ± 0.3	300.9 ± 0.2
2014-SH 21 hr	29.4 ± 5.1	359.6 ± 9.2	17.9 ± 1.0	318.8 ± 2.9	31.0 ± 1.7	383.1 ± 9.3	33.3 ± 0.1	392.2 ± 1.3
2014-SH 00 hr	21.9 ± 4.9	326.1 ± 3.3	10.2 ± 0.5	313.1 ± 1.3	24.9 ± 2.7	338.6 ± 9.1	28.2 ± 0.2	350.9 ± 1.4
2014-SH 03 hr	18.1 ± 3.2	318.5 ± 3.4	8.8 ± 0.2	298.8 ± 2.2	21.7 ± 2.0	321.7 ± 6.5	23.2 ± 0.3	338.3 ± 0.6

NH (green line) and SH (black line) during 2011; the average vTEC variation in the NH (green line) and SH (black line) during 2014; the F10.7A (red line) and the h_mF_2 in the NH (green line) and SH (black line) during 2014; and the meridional wind velocity in the NH (green line) and SH (black line). The HWM-14 model was employed to approximate the meridional wind velocity. As was previously indicated, however, somo models of ionospheric parameters, such as HWM-14, are restricted to quiet solar activity conditions; hence, only one variation plot of meridional wind velocity (labeled as "merdl") was included for the two years (as seen in Figure 7, panel 5). The h_mF_2 was approximated using the International Reference Ionosphere (IRI2001) model, using Chapman model parameters.

Theoretically, geomagnetic conjugate points are defined as two points on Earth's surface, connected by a magnetic field line. It means that the effects on the plasma at these points caused by the neutral wind drag would be linked and, consequently, could be reflected as a change in the h_mF_2 ($\Rightarrow$ change in the recombination processes) and the electron density. In this case, comparing the two average vTEC trends, representing the NH and SH electron density variation, an hemispheric asymmetry of semiannual anomaly can be distinguished. Two ionization crests are identified in the SH, while in the NH, just one ionization crest in March–April is observed in 2014. As the yellow bars indicate, these ionizations crests occurred at different time in each hemisphere (as seen in panels 2 and 4 in Figure 7), which makes the disparity between the two hemispheres more evident.

For 2011, the vTEC variation in the NH was quasi-constant from April to October, showing minimal differences between the two ionization crests. Comparing this vTEC variation with the h_mF_2, we observed that the F_2 layer moved to the highest altitudes from April to September and also exhibited a constant behavior (~324 ± 2.5 km). This behavior is congruent with the vTEC trend since, as we mentioned before, the recombination rate in the ionosphere is controlled by the h_mF_2; when the h_mF_2 decreases, the recombination rate becomes higher, and, hence, the electron density diminishes. In this case, the F_2 layer remained at the same altitude, and then the electron density was also constant. According to the HWM-14 approximations, the meridional wind in the NH was moving southward (equatorward wind) with a quasi-constant velocity from April to October, a period that presented the highest values (approximately −40 m/s). It suggests that the plasma, following the magnetic field lines, may be displaced to higher altitudes by the effect of this equatorward wind. This upward movement of the plasma is also congruent with the highest h_mF_2 registered in these months. To complement the analysis of the electron density variation in terms of the h_mF_2, Table 3 reports a comparison between the vTEC values and the average of h_mF_2 during March–April, June–July, October–November, and December at 21:00, 00:00, and 03:00 a.m. LT. Here, we observed that the highest vTEC values registered during March–April and June–July of 2011 were associated with the highest values of h_mF_2, which reinforces the behavior observed in Figure 7 (see panels 1 and 2).

On the other hand, in the SH, we found that the vTEC trend was very similar to that observed in the daytime. The two ionization crests were well defined in March and November in 2011. According to HMW-14 approximations, the highest velocities of the meridional winds (~72 ± 7 m/s) were registered in the SH from January to March and from November to December. During these periods, the wind was moving to the north (equatorward winds), which suggests an upward movement of the *F* layer to heights where the plasma experiences a lower recombination that makes the plasma live longer. Such an ascension can be supported by the approximations in Figure 7 and Table 3, in which the higher values of h_mF_2 (over 320 km) were registered during March, November, and December. The minimum of vTEC observed in June–July coincides with a period in which the meridional wind velocity was 0 m/s. It suggests that the F_2 layer remained at a low altitude (~292 km), where the plasma recombination was higher than in comparison with the other altitudes registered. It is important to highlight that the altitude of the F_2 layer decreased as the night progresses, which can be associated with the attenuation of the seasonal vTEC trend (see Table 3 and Figure 5).

Figure 7 also corroborates the presence of strong equatorward winds in the SH during January and December (~100 m/s). As we mentioned in section 2, such equatorward winds, in conjunction with the EIA fountain effect, may help to explain the formation of the MSNA. Although the equatorward winds had the same velocity in these 2 months, however, the magnitude of the MSNA, in terms of the DTEC, was lower in December than in June, even though December presented a more robust EIA signature. Observing the daytime vTEC maps, we note that the weak MSNA during December was caused by the significant difference of vTEC between January and December (January 2011 $= 22.8 \pm 2.0$ TECu; December 2011 $= 43.4 \pm 4.5$ TECu). Thus, although vTEC enhancement seems to be stronger in December than in January in the maps of Figure 1, the plasma distribution during the daytime determines the magnitude of the MSNA. Furthermore, Lin et al. (2010) reported that the MSNA is also visible near to the June solstice, but in this case such a period coincides with the absence of the EIA and very low equatorward wind velocity. For that reason, the MSNA was not observed during 2011.

For 2014, in the NH, the vTEC trend exhibited just one ionization crest around April. In this case, such a trend does not seem to be correlated with the h_mF_2 variation and meridional wind profile. Although for 2011, the vTEC trend and hemispheric asymmetries may be attributed to the asymmetries of the meridional wind component, the limitations of the HWM-14 (no differences between distinct years) did not allow infering about the effect of meridional winds during 2014. Nonetheless, these results suggest that nighttime equatorward winds are the main responsibles factors for the seasonal vTEC variation, and the absence of semiannual and seasonal anomaly in the NH. As Zou et al. (2000) explained, the equatorward winds modulate the electron density distribution at night.

4. Conclusions

We presented the analysis of nighttime vTEC variations over Latin America. Geomagnetically undisturbed days of 2011 and 2014, associated with two different phases of Solar Cycle 24, were examined in order to analyze the solar activity influences, seasonal variations, and hemispheric asymmetries of vTEC. With this purpose, we used data from a set of GNSS receivers of the networks SSN-TLALOCNet (Mexico), COCONet (Central America), RBMC (Brazil), RAMSAC (Argentina), and IGS (South America). The vTEC values, estimated using the methodology of Embrace/INPE, were utilized to construct the vTEC variation curves and vTEC maps at 21:00, 00:00, and 03:00 LT.

The Latin American region includes ionospheric characteristics of equatorial, low, and middle latitudes, where spatial and temporal electron density variations coexist. Thus, the plasma distribution shown on the vTEC maps reflects the ionosphere dynamics over this region, which has been discussed in terms of the meridional wind and the average h_mF_2. The main results obtained from this qualitative and quantitative analysis are summarized bellow.

- Important differences in the seasonal TEC trend at low, equatorial, and middle latitudes were observed, revealing a strong latitudinal dependence. At 21:00 LT, the nighttime seasonal trend of vTEC seems to be a residual effect from that observed in the daytime. After midnight, however, receivers at equatorial and low latitudes showed a different seasonal trend.
- The semiannual anomaly had a different configuration in each hemisphere. The ionization crests occurred at a different time in each hemisphere. They were observed in April–May and

October–November in the NH, while in the SH, they occurred in March and November. In addition, during 2014, this anomaly was absent for midlatitude receivers in the NH.

- The EIA presented a seasonal behavior similar to the vTEC trend. It means the EIA signature was more robust during the months associated with the ionization crests: April and November for 2011 and March and November for 2014. The EIA signature was absent from June to August, a period in which the hemispheric disparity in the vTEC values became more evident than in the other months. Especially for June, the coincidence of the highest values of vTEC with the summer hemisphere suggests a feeble interhemispheric circulation.
- The MSNA was identified in the SH during January and February of 2011 (moderate solar activity). According to the HWM-14 approximations, such a period coincides with the presence of strong equatorward winds. The interaction of these equatorward winds with the downward plasma fluxes caused by the fountain effect may be responsible for the increase of the electron density at midlatitudes. Further observations, however, are needed to corroborate this fact. In addition, the intensity of this anomaly diminished with the night progresses, becoming imperceptible at 03:00 a.m. LT.
- The seasonal variability of the ionosphere over this region, including the MSNA, the EIA, and the annual anomaly, was no longer significant after midnight.
- In general, the HWM-14 model approximations suggested that the equatorward winds had a strong influence on nighttime vTEC variations during these periods. Although the limitations of this model (no differences between distinct solar activity phases) did not allow inferring about the effect of these winds during 2014.

Data Aailability Statement

The authors thank Embrace/INPE for supporting the GNSS data analysis methodology (https://www2.inpe.br/climaespacial/portal/tec-map-home/), the World Data Center for Geomagnetism, Kyoto, for the AE and Dst indices data (https://wdc.kugi.kyoto-u.ac.jp/wdc/Sec3.html), and NOAA for the Kp index and solar radio flux data (//ftp.swpc.noaa.gov/pub/indices/). The GNSS ground-based receiver data were collected from different GNSS networks in South America: RBMC from IBGE (https://www.ibge.gov.br/geociencias/informacoes-sobre-posicionamento-geodesico/rede-geodesica/16258-rede-brasileira-de-monitoramento-continuo-dos-sistemas-gnss-rbmc.html?=&t=downloads); RAMSAC of Argentina (https://www.ign.gob.ar/NuestrasActividades/Geodesia/Ramsac/DescargaRinex), IGS (https://kb.igs.org/hc/en-us/articles/201096516-IGS-Formats); and in Central America COCONET (https://coconet.cimh.edu.bb/coconetgsac/gsacapi/file/form). We thank these network sites for providing continuous data. GPS Rinex data for the Mexican region were obtained from the following GPS permanent networks: the Mexican Servicio Sismológico Nacional (SSN), IGEF-UNAM, SSN-TLALOCNet and TLALOCNet (https://tlalocnet.udg.mx/tlalocnetgsac/gsacapi/file/form). We thank the LACIGE-UNAM at ENES unidad Morelia for the data provided by the GPS receiver, acquired through the infrastructure CONACyT Grant 253691 and also the UNAM-PAPIIT projects IA 107116 and IN 118119.

Acknowledgments
E. Romero-Hernandez thanks all coauthors for helping in the development of this work. C. M. Denardini thanks CNPq/MCTIC (Grant 303643/2017-0). J. A. González-Esparza acknowledges support from CONACyT LN 293598, CONACYT PN 2015-173, CONACyT-AEM 2017-01-292684, and DGAPA-PAPIIT IN106916. L. C. A. Resende would like to thank the China-Brazil Joint Laboratory for Space Weather (CBJLSW), National Space Science Center (NSSC), and the Chinese Academy of Sciences (CAS) for supporting her postdoctoral project. E. Aguilar-Rodriguez thanks DGAPA-PAPIIT project, Grant IN101718. O. F. Jonah acknowledges support from NSF Grant AGS-1242204 from the Massachusetts Institute of Technology. V. De la Luz thanks CONACyT Ciencia Basica (254497) fellowship. G. A. S. Picanço thanks Capes/MEC (Grant 88887.351778/2019-00). The calculations of the local TEC values are partly based on GPS data provided by the Servicio Sismológico Nacional (SSN, 2018; Pérez-Campos et al., 2018) and the Trans-boundary, Land and Atmosphere Long-term Observational and Collaborative Network (TLALOCNet; Cabral-Cano et al., 2018) and SSN-TLALOCNet operated by the Servicio de Geodesia Satelital (SGS) and SSN at the Instituto de Geofísica-Universidad Nacional Autonoma de Mexico (UNAM) and UNAVCO Inc. We gratefully acknowledge all the personnel from SSN, SGS, and UNAVCO Inc. for station maintenance, data acquisition, IT support, and data distribution for these networks. TLALOCNet, SSN-TLALOCNet, and related SGS operations are supported by the National Science Foundation Number EAR-1338091; NASA-ROSES NNX12AQ08G; CONACyT projects 253760, 256012, and 2017-01-5955; DGAPA-PAPIIT projects IN104213, IN111509, IN109315-3, and IN104818-3; and supplemental support from UNAM-Instituto de Geofísica and Centro de Ciencias de la Atmosfera.

References

Abdu, M. A. (2005). Equatorial ionosphere-thermosphere system: Electrodynamics and irregularities. *Advances in Space Research*, *35*, 771–787.

Balan, N., Otsuka, Y., Fukao, S., Abdu, M. A., & Bailey, G. J. (2000). Annual variations of the ionosphere: A review based on MU radar observations. *Advances in Space Research*, *25*(1), 153–162. https://doi.org/10.1016/S0273-1177(99)00913-8

Balan, N., Souza, J., & Bailey, J. G. (2018). Recent developments in the understanding of equatorial ionization anomaly: A review. *Journal of Atmospheric and Solar-Terrestrial Physics*, *171*, 3–11. https://doi.org/10.1016/j.jastp.2017.06.020

Buonsanto, M. (1999). Ionospheric storms—A review. *Space Science Reviews*, *88*, 563–601. https://doi.org/10.1023/A:1005107532631

Chen, Y., Liu, L., & Le, H. (2008). Solar activity variations of nighttime ionospheric peak electron density. *Journal of Geophysical Research*, *113*, A11306. https://doi.org/10.1029/2008JA013114

Chen, Y., Liu, L., Wan, W., & Ren, Z. (2012). Equinoctial asymmetry in solar activity variations of NmF2 and TEC. *Annales Geophysicae*, *30*, 613–622. https://doi.org/10.5194/angeo-30-613-2012

Drob, D. P., Emmert, J. T., Meriwether, J. W., Makela, J. J., Doornbos, E., Conde, M., et al. (2015). An update to the Horizontal Wind Model (HWM): The quiet time thermosphere. *Earth and Space Science*, *2*, 301–319. https://doi.org/10.1002/2014EA000089

Fang, T. W., Akmaev, R., Fuller-Rowell, T., Wu, F., Maruyama, N., & Millward, G. (2013). Longitudinal and day-to-day variability in the ionosphere from lower atmosphere tidal forcing. *Geophysical Research Letters*, *40*, 2523–2528. https://doi.org/10.1002/grl.50550

Foster, M., & Jakowski, N. (1988). The Nighttime Winter Anomaly (NWA) effect in the American sector as a consequence of interhemispheric ionospheric coupling. *PAGEOPH*, *127*, 447–471. https://doi.org/10.1007/BF00879821

Fritts, D. C., Abdu, M. A., Batista, B. R., Batista, I. S., et al. (2013). Overview and summary of the Spread F Experiment (spreadFEx). *Annales Geophysicae*, *27*, 2141–2155.

Fuller-Rowell, T (1998). The thermospheric spoon: A mechanism for the semiannual density variation. *Journal of Geophysical Research*, *103*(A3), 3951–3956.

Fuller-Rowell, T. J., Codrescu, M. V., Roble, R. G., & Richmond, A. D. (1997). How does the thermosphere and ionosphere react to a geomagnetic storm? In B. T. Tsurutani, W. D. Gonzalez, Y. Kamide, J. K. Arballo (Eds.), *Magnetic Storms, Geophysical Monograph Series* (Vol. 98, pp. 203–225). Washington, DC: American Geophysical Union. https://doi.org/10.1029/GM098p0203

Jakowski, N., Hoque, M. M., Kriegel, M., & Patidar, V. (2015). The persistence of the NWA effect during the low solar activity period 2007–2009. *Journal of Geophysical Research: Space Physics*, *120*, 9148–9160. https://doi.org/10.1002/2015JA021600

Jee, G., Schunk, R. W., & Scherliess, L. (2005). On the sensitivity of total electron content (TEC) to upper atmospheric/ionospheric parameters. *Journal of Atmospheric and Solar-Terrestrial Physics*, *67*, 1040–1052.

Jonah, O. F., de Paula, E. R., Muella, M. T. A. H., Dutra, S. L. G., Kherani, E. A., Negreti, P. M. S., & Otsuka, Y. (2015). TEC Variation during high and low solar activities over South American sector. *Journal of Atmospheric and Solar-Terrestrial Physics*, *135*, 22–35. https://doi.org/10.1016/j.jastp.2015.10.005

Lee, W. K., Kil, H., Kwak, S., Wu, Q., Cho, S., & Park, J. U. (2011). The winter anomaly in the middle-latitude F region during the solar minimum period observed by the Constellation Observing System for Meteorology, Ionosphere, and Climate. *Journal of Geophysical Research*, *116*, A02302. https://doi.org/10.1029/2010JA015815

Lin, C. H., Liu, J. Y., Fang, T. W., Chang, P. Y., Tsai, H. F., Chen, C. H., & Hsiao, C. C. (2007). Motions of the equatorial ionization anomaly crests imaged by FORMOSAT-3/ COSMIC. *Geophysical Research Letter*, *2007*, L9101. https://doi.org/10.1029/2007GL030741

Lin, C. H., Liu, C. H., Liu, J. Y., Chen, C. H., Burns, A. G., & Wang, W. (2010). Midlatitude summer nighttime anomaly of the ionospheric electron density observed by FORMOSAT3/COSMIC. *Journal of Geophysical Research*, *115*, A03308. https://doi.org/10.1029/2009JA014084

Liu, L., Wan, W., Ning, B., Pirog, O. M., & Kurkin, V. I. (2006). Solar activity variations of the ionospheric peak electron density. *Journal of Geophysical Research*, *111*, 8304. https://doi.org/10.1029/2006JA011598

Liu, L., Wan, W., Ning, B., & Zhang, M.-L. (2009). Climatology of the mean total electron content derived from GPS global ionospheric maps. *Journal of Geophysical Research*, *114*, A06308. https://doi.org/10.1029/2009JA014244

Liu, H. L., Yudin, V. A., & Roble, R. G. (2013). Day-to-day ionospheric variability due to lower atmosphere perturbations. *Geophysical Research Letters*, *40*, 665–670. https://doi.org/10.1002/GRL.50125

Lyon, A. J., & Thomas, L. (1963). The F_2-region equatorial anomaly in the African, American and East Asian sectors during sunspot maximum. *Journal of Atmospheric and Solar-Terrestrial Physics*, *1963*(25), 373–386. https://doi.org/10.1016/0021-9169(63)90170-3

Mannucci, A. J., Wilson, B. D., Yuan, D. N., Ho, C. H., Lindqwister, U. J., & Runge, T. F. (1998). A global mapping technique for GPS-derived ionospheric total electron content measurements. *Radio Science*, *33*(3), 565–582. https://doi.org/10.1029/97RS02707

McDonald, S. E., Dymond, K. F., & Summers, M. E. (2008). Hemispheric asymmetries in the longitudinal structure of the low-latitude night time ionosphere. *Journal of Geophysical Research*, *113*, A08308. https://doi.org/10.1029/2007JA012876

Medeiros, R. T., Abdu, M. A., & Batista, I. S. (1997). Thermospheric meridional wind at low latitude from measurements of F layer peak height. *Journal of Geophysical Research*, *1997*(102), 14,531–14,540.

Otsuka, Y., et al. (2002). A new technique for mapping of total electron content using GPS network. *Earth Planets Space*, *54*, 63–70. https://doi.org/10.1186/BF03352422

Qian, L., Burns, A. G., Wang, W., Solomon, S. C., Zhang, Y., & Hsu, V (2016). Effects of the equatorial ionosphere anomaly on the interhemispheric circulation in the thermosphere. *Journal of Geophysical Research: Space Physics*, *121*, 2522–2530. https://doi.org/10.1002/2015JA022169

Rama Rao, P. V. S., Gopi Krishna, S., Niranjan, K., & Prasad, D. S. V. V. D (2006). Temporal and spatial variations in TEC using simultaneous measurements from the Indian GPS network of receivers during the low solar activity period of 2004-2005. *Annales Geophysicae*, *24*(12), 3279–3292. https://doi.org/10.5194/angeo-24-3279-2006

Rishbeth, H., & Mendillo, M. (2001). Patterns of F_2-layer variablility. *Journal of Atmospheric and Solar-Terrestrial Physics*, *2001*(63), 1661–1680.

Romero-Hernandez, E., Denardini, C. M., Takahashi, H., Gonzalez-Esparza, J. A., Nogueira, P. A. B., de Pádua, M. B., et al. (2018). Daytime ionospheric TEC weather study over Latin America. *Journal of Geophysical Research: Space Physics*, *121*, 10,345–10,357. https://doi.org/10.1029/2018JA025943

Sai Gowtam, V., & Tulasi Ram, S. (2017). Ionospheric winter anomaly and annual anomaly observed from Formosat-3/COSMIC Radio Occultation observations during the ascending phase of Solar Cycle 24. *Advances in Space Research*, *60*, 1585–1593. https://doi.org/10.1016/j.asr.2017.03.017

Sergeeva, M. A., Maltseva, O. A., Gonzalez-Esparza, J. A., Mejia-Ambriz, J. C., De la Luz, V., Corona-Romero, P., et al. (2018). TEC behavior over the Mexican region. *Annals of Geophysics*, *61*(1), GM104. https://doi.org/10.4401/ag-7

Takahashi, H., Wrasse, C. M., Denardini, C. M., Pádua, M. B., de Paula, E. R., Costa, S. M. A., et al. (2016). Ionospheric TEC weather map over South America. *Space Weather*, *14*, 937–949. https://doi.org/10.1002/2016SW001474

Thampi, S. V., Balan, N., Lin, C., Liu, H., & Yamamoto, M (2011). Mid-latitude Summer Nighttime Anomaly (MSNA)—Observations and model simulations. *Annales Geophysicae*, *29*, 157–165. https://doi.org/10.5194/angeo-29-157-2011

Tsai, H.-F., Liu, J.-Y., Tsai, W.-H., Liu, C.-H., Tseng, C.-L., & Wu, C.-C. (2001). Seasonal variations of the ionospheric total electron content in Asian equatorial anomaly regions. *Journal of Geophysical Research*, *106*(A12), 30,363–30,369. https://doi.org/10.1029/2001JA001107

Tsugawa, T., Zhang, S. R., Coster, A. J., Otsuka, Y., Sato, J., Saito, A., et al. (2007). Summer-winter hemispheric asymmetry of the sudden increase in ionospheric total electron content and of the O/N2 ratio: Solar activity dependence. *Journal of Geophysical Research*, *112*, A08301. https://doi.org/10.1029/2007JA012415

Unnikrishnan, K., Balanchandran Nair, R., & Venugopal, C. (2002). A comparative study of night-time enhancement of TEC at a low latitude station on storm and quiet nights including the local time, seasonal and solar activity dependence. *Annales Geophysicae*, *20*, 1843–1850.

Unnikrishnan, K., Saito, A., & Fukao, S. (2006). Differences in daytime and nighttime ionospheric deterministic chaotic behavior: GPS total electron content. *Journal of Geophysical Research*, *111*, A07310. https://doi.org/10.1029/2005JA011313

Yizengaw, E., Moldwin, M. B., Sahai, Y., & de Jesus, R. (2009). Strong postmidnight equatorial ionospheric anomaly observations during magnetically quiet periods. *Journal of Geophysical Research*, *114*, A12308. https://doi.org/10.1029/2009JA014603

Zhao, B., Wan, W., Liu, L., Mao, T., Ren, Z., Wang, M., & Christensen, A. B. (2008). Features of annual and semiannual variations derived from the global ionospheric maps of total electron content. *Annales Geophysicae*, *25*, 2513–2527.

Zou, L., Rishbeth, H., Mulle-Wodarg, I. C. F., Aylward, A. D., Millward, G. H., Fulle-Rowell, T. J., et al. (2000). Annual and semiannual variations in the ionospheric F_2-layer. I. Modelling. *Annales Geophysicae*, *18*, 927–944.